Design and Characterization of a Novel Intravitreal Dual-Transgene Genetic Medicine for Neovascular Retinopathies

Melissa A. Calton,[1] Roxanne H. Croze,[1] Christian Burns,[1] Ghezal Beliakoff,[1] Tandis Vazin,[1] Paul Szymanski,[1] Christopher Schmitt,[1] Austin Klein,[1] Meredith Leong,[1] Melissa Quezada,[1] Jenny Holt,[1] Gabe Bolender,[1] Katherine Barglow,[1] Devi Khoday,[1] Thomas Mason,[1] Katherine Delaria,[1] Mohammad Hassanipour,[1] Melissa Kotterman,[1] Arshad M. Khanani,[2,3] David Schaffer,[4] Peter Francis,[1] and David Kirn[1,4]

[1]4D Molecular Therapeutics, Emeryville, California, United States
[2]Sierra Eye Associates, Reno, Nevada, United States
[3]University of Nevada, Reno School of Medicine, Reno, Nevada, United States
[4]University of California, Berkeley, California, United States

Correspondence: David Kirn, 4D Molecular Therapeutics, 5858 Horton Street, Emeryville, CA 94608, USA;
dkirn@4dmt.com.

Received: June 3, 2024
Accepted: October 28, 2024
Published: December 2, 2024

Citation: Calton MA, Croze RH, Burns C, et al. Design and characterization of a novel intravitreal dual-transgene genetic medicine for neovascular retinopathies. *Invest Ophthalmol Vis Sci.* 2024;65(14):1. https://doi.org/10.1167/iovs.65.14.1

Purpose. Intravitreal delivery of therapeutic transgenes to the retina via engineered viral vectors can provide sustained local concentrations of therapeutic proteins and thus potentially reduce the treatment burden and improve long-term vision outcomes for patients with neovascular (wet) age-related macular degeneration (AMD), diabetic macular edema (DME), and diabetic retinopathy.

Methods. We performed directed evolution in nonhuman primates (NHP) to invent an adeno-associated viral (AAV) variant (R100) with the capacity to cross vitreoretinal barriers and transduce all regions and layers of the retina following intravitreal injection. We then engineered 4D-150, an R100-based genetic medicine carrying 2 therapeutic transgenes: a codon-optimized sequence encoding aflibercept, a recombinant protein that inhibits VEGF-A, VEGF-B, and PlGF, and a microRNA sequence that inhibits expression of VEGF-C. Transduction, transgene expression, and biological activity were characterized in human retinal cells in vitro and in NHPs.

Results. R100 demonstrated superior retinal cell transduction in vitro and in vivo compared to AAV2, a commonly used wild-type AAV serotype in retinal gene therapies. Transduction of human retinal pigment epithelial cells in vitro by 4D-150 resulted in dose-dependent transgene expression and corresponding reductions in VEGF-A and VEGF-C. Intravitreal administration of 4D-150 to NHPs was well tolerated and led to robust retinal expression of both transgenes. In a primate model of laser-induced choroidal neovascularization, 4D-150 completely prevented clinically relevant angiogenic lesions at all tested doses.

Conclusions. These findings support further development of 4D-150. Clinical trials are underway to establish the safety and efficacy of 4D-150 in individuals with wet AMD and DME.

Keywords: wet age-related macular degeneration (AMD), gene therapy, intravitreal injection, aflibercept, VEGF, placental growth factor (PlGF), directed evolution

Age-related macular degeneration (AMD) accounts for nearly 10% of all blindness worldwide and represents the most common cause of irreversible blindness in developed countries.[1,2] In neovascular (wet) AMD, choroidal neovascularization (CNV) manifests as uncontrolled growth of leaky blood vessels under the macula and accumulation of fluid within and beneath the retina, causing macular edema and progressive degeneration of photoreceptors and retinal pigment epithelium (RPE).[3,4] In diabetic macular edema (DME), retinal vascular abnormalities caused by hyperglycemia compromise the integrity of the blood-retinal barrier, resulting in increased vascular permeability, intraretinal fluid accumulation, and progressive retinal dysfunction.[5,6]

Repeated intravitreal (IVT) injections of anti-VEGF therapies effectively slow vision loss in the majority of treatment-compliant patients with wet AMD.[7–13] However, the requirement for lifelong injections imposes a substantial burden on patients and caregivers, and many patients fail to maintain initial therapeutic benefits owing to noncompliance with the burdensome treatment regimen.[3,7,8,10,13–20] In addition, no approved therapy for wet AMD targets VEGF-C,

a potentially important target and driver of treatment resistance.[21–24]

Gene therapy delivered directly to the retina via viral vectors has the potential to provide a durable benefit and reduce the treatment burden for patients with retinal diseases. Adeno-associated virus (AAV) vectors are the leading platform for the delivery of in vivo gene therapy; however, IVT delivery of therapeutic transgenes to multiple cell types across the entire retina has not been feasible with wild-type AAV vectors owing in part to their limited capacity to efficiently transit the vitreous and penetrate the inner limiting membrane (ILM) and superficial ganglion cell layer.[25] As a consequence, wild-type AAV-based gene therapies for ophthalmologic indications generally require relatively high doses and/or administration via subretinal injection, an invasive surgical procedure that requires detachment of photoreceptors from the RPE and reportedly results in transduction of <5% of the retinal surface.[25–27]

We implemented a directed evolution strategy that used genetic diversification and selection processes to invent a novel AAV capsid (R100) with the capacity to transduce all major cell types across all regions of the primate retina, including the macula, following IVT administration at relatively low doses. We then designed and engineered 4D-150, a dual-transgene genetic medicine comprising the R100 vector and a transgene expression cassette containing: (1) a codon-optimized sequence encoding aflibercept, a clinically validated recombinant chimeric protein that binds VEGF-A, VEGF-B, and placental growth factor (PlGF), and (2) a microRNA (miRNA) sequence that inhibits intracellular expression of VEGF-C (miR-VEGF-C). Here, we describe the design and preclinical characterization of the R100 synthetic AAV capsid, and the R100-based gene therapy candidate 4D-150.

Methods

All animal experiments were conducted in accordance with the Association for Research in Vision and Ophthalmology Statement for the Use of Animals in Ophthalmic and Vision Research. All animal studies were conducted under protocols approved by the institutional animal care and use committees overseeing animal welfare at the Valley Biosystems, CRL, and Virscio facilities. Experimental methods are described briefly below. A comprehensive description of methods and materials is provided in the Supplementary Material.

Vector Discovery

Detailed methods for the in vivo directed evolution process are described in the Supplementary Methods. Briefly, a pooled library of approximately 10^8 unique synthetic variant AAV capsid sequences was created from 25 different sub-libraries using various molecular biology techniques and packaged in HEK293T cells to produce DNA-containing capsids. Each unique capsid protein is encoded by the DNA sequence that is carries (Fig. 1A).[28–35] The resulting capsid library was administered by IVT injection to a NHP and subjected to in vivo selective pressures to mimic IVT clinical gene therapy. All synthetic libraries were injected in the first round of selection. Genomes were recovered from retina tissue harvested from each quadrant (superior, inferior, nasal, and temporal) and from each of four cell layers (RPE, outer nuclear layer, inner nuclear layer, and ganglion cell layer). Recovered genomes were amplified and packaged for injection into another NHP. This procedure was repeated for a total of six cycles. To increase the stringency of selection, progressively lower quantities of viral particles were administered in each successive cycle. Additional mutagenesis techniques were applied to recovered capsid sequences between rounds four and five to increase diversity. After each round from three to six, sequencing was performed on individual clones isolated from targeted retinal tissues to determine the prevalence of variants and sequence motifs within the remaining capsid population. A "hit" was defined as a variant with a prevalence of ≥5% of the total sequenced population in two or more consecutive rounds of selection or ≥10% of the total sequenced population in one or more rounds.

DNA was isolated from tissue samples using the QIAamp DNA Mini isolation kit (Qiagen, Hilden, Germany). AAV variant *cap* genes were amplified by PCR and inserted into the pSub2 library packaging plasmid, as previously described.[29,30,32,34] *Cap* genes were sequenced by third-party DNA sequencing facilities and analyzed using Geneious software (Biomatters, Aukland, New Zealand). Peptide homology was assessed using the protein-protein basic local alignment search tool.

Cell Culture

HEK293T and HEK293 cells were cultured in DMEM supplemented with 4% to 10% FBS. Human embryonic stem cells (ESI-017) and human fibroblast-derived induced pluripotent stem cells (FB-iPSCs) were cultured on Matrigel (Corning, Glendale, AZ, USA) in mTeSR-1 maintenance medium (Stem Cell Technologies, Vancouver, British Columbia, Canada). Human pluripotent stem cell (hPSC) cultures were subcultured using Gentle Cell Dissociation Reagent (Stem Cell Technologies) every 4 to 5 days at 70% to 80% confluence. Human vascular endothelial cells (HUVEC) were cultured in an endothelial basal medium (EBM-2; Lonza, Basel, Switzerland) according to the manufacturer's instructions. Hap1 cells were cultured in Iscove's modified Dulbecco's medium (Gibco) supplemented with 10% FBS and 1% penicillin/streptomycin (ThermoFisher, Waltham, MA, USA).

In Vivo Vector Characterization

Vector characterization studies were performed in 2 nonhuman primate (NHP) species with the R100 capsid carrying an enhanced green fluorescent protein (EGFP) reporter transgene. Cynomolgus macaques (age = 2–8 years) received bilateral IVT injections of R100.CAG-EGFP (3×10^{11} vg/eye or 1×10^{12} vg/eye) (Supplementary Table S1). Adult African green monkeys received either R100.CMV-EGFP or AAV2.CMV-EGFP (2×10^{11} vg/eye) via IVT injection. All animals were screened for pre-existing neutralizing antibodies to R100 and AAV2. In-life EGFP expression was assessed by fundus fluorescence imaging.[36–39] Animals received immunosuppression with methylprednisolone and/or IVT triamcinolone (Supplementary Methods). In the cynomolgus macaque studies, animals were euthanized and selected eyes were enucleated and fixed in 4% paraformaldehyde and stored in 30% sucrose at 4°C. The retina was dissected into superior, inferior, temporal, nasal, and optic nerve/fovea/macula regions and individually mounted in optimum cutting temperature mounting medium.

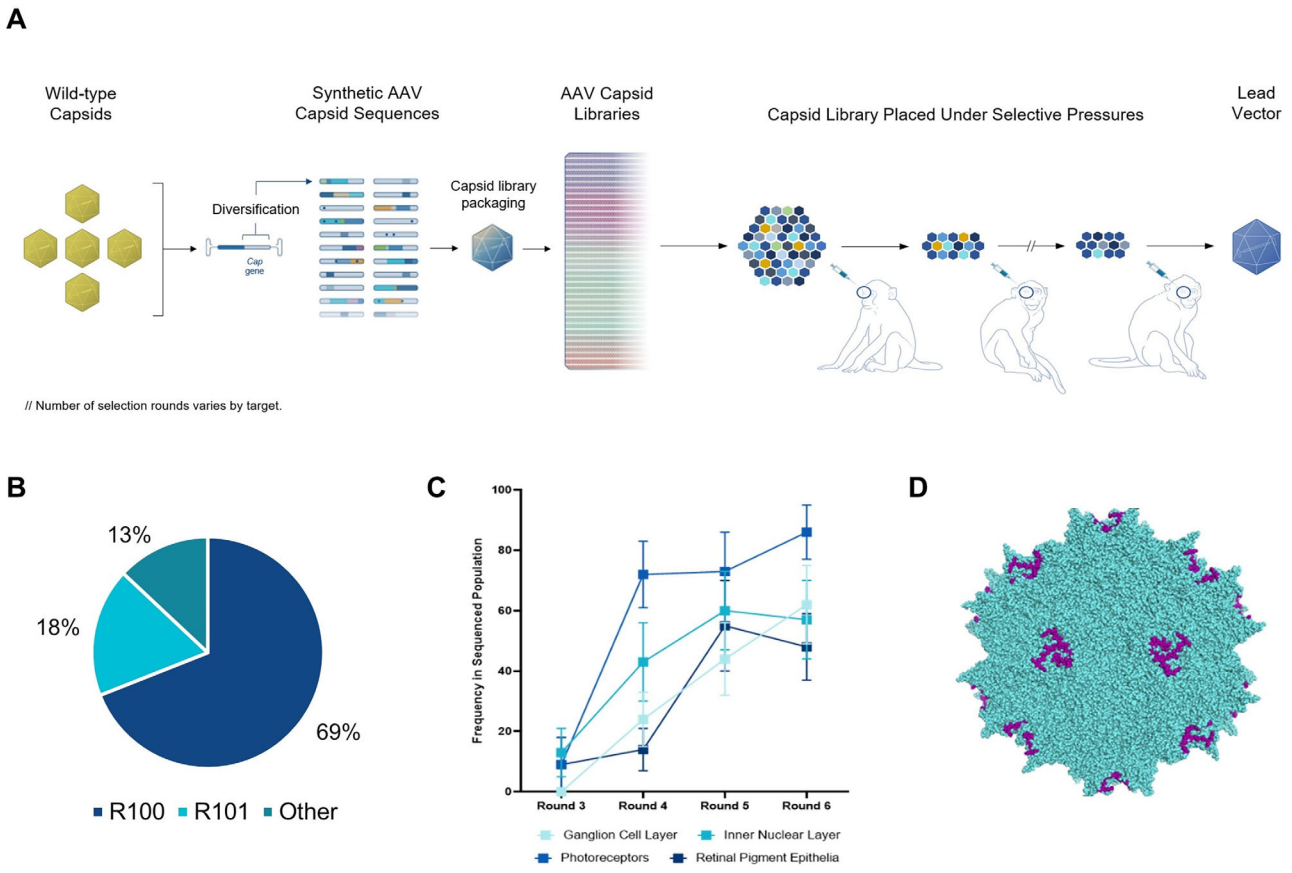

Figure 1. Directed evolution of AAV capsid in primates led to the discovery of a dominant capsid variant (R100). (**A**) Schematic representation of directed evolution. A plasmid library comprising synthetic variant AAV capsid sequences is created from the *cap* genes of several wild-type AAV serotypes using various DNA mutation techniques. The library is packaged in HEK293T cells to produce viral particles comprising a synthetic capsid shell surrounding the viral capsid genome. The viral library is then purified and subjected to in vivo selective pressures. Successful viruses are amplified, recovered, and enriched through repeated rounds of selection. (**B**) Frequency of the top two capsid variants in the directed evolution round six sequencing analysis. (**C**) Frequency of the R100 variant motif found in separate retinal cell layers in directed evolution rounds three to six. Error bars indicate 95% confidence intervals. (**D**) Representative 3D model of R100. The AAV2-based variant contains an insertion of 10 amino acids (*purple*) at amino acid position 588. AAV, adeno-associated virus.

The slides were permeabilized and blocked with blocking buffer (PBS with 0.5% Triton X-100 and 10% goat serum) and incubated overnight with primary antibodies (Supplementary Table S2) in blocking buffer at 4°C. The slides were then washed and incubated with Alexa Fluor-conjugated secondary antibodies (see Supplementary Table S2) for 1 hour at room temperature in blocking buffer. Tissues were counterstained with DAPI nuclear stain. Images were acquired using a Zeiss Axio Observer Z1 or D1 microscope. For tiling, sequential multichannel images with approximately 5% overlap were acquired. Images were processed using Zen Blue 2.3 and FIJI Image J software.

Acute Retinal Biodistribution of 4D-150

Cynomolgus macaques (age = 6 years) received bilateral IVT injections of 4D-150 1×10^{12} vg/eye. Methylprednisolone was administered via intramuscular (IM) injection on day –1 and then once weekly; a single IVT injection of triamcinolone 2 mg was administered on day 1. Aqueous and vitreous humor samples were collected separately from both eyes 4 weeks post injection and stored at ≤–70°C. Retinal tissue samples were dissected into superior, nasal, central, temporal, and inferior regions, then placed individually in RNAlater solution, and stored at ≤–20°C.

Retina and choroid samples were homogenized in tissue lysis buffer (250 mM HEPES, 150 mM NaCl, 1% Triton X-100, and 5 mM EDTA, 1 × protease and phosphatase inhibitor cocktail), incubated on ice, and clarified by centrifugation. Free aflibercept was evaluated using the aflibercept ELISA kit (Cat. No. IG-AA115; Eagle Biosciences, Nashua, NH, USA). Mature miRNA in retinal tissue was quantified by reverse transcription quantitative PCR (RT-qPCR). Total RNA was isolated from retinal tissues using a miRNeasy kit (Qiagen, protocol #74104).

Safety and Efficacy of 4D-150

The safety and efficacy of 4D-150 were evaluated in a primate laser-induced CNV assay. The assay recapitulates the main features of the exudative form of human AMD (see Supplementary Methods).[40] Male and female African green monkeys (age = 4–13 years) were randomly assigned to receive bilateral IVT injections of 4D-150 (1×10^{11}, 3×10^{11}, or 1×10^{12} vg/eye), R100.CAG-AFLB (1×10^{12} vg/eye), or vehicle. Methylprednisolone IM was administered on day –1 and then once weekly for 4 weeks. A single dose of triam-

Investigative Ophthalmology & Visual Science

cinolone 2 mg was administered via subtenon injection on day 1 following administration of the test article. Three days prior to laser photocoagulation, all animals received bilateral subconjunctival injections of dexamethasone 1 mg. At day 42, six laser spots were placed within the perimacular region in each eye using an Iridex Oculight TX 532-nm laser (duration = 100 ms, spot size = 50 µm, and power = 750 mW). Color fundus photography was performed immediately after laser treatment using a Topcon TRCS0EX retinal camera with Canon 6D digital imaging hardware and New Vision Fundus Image Analysis System software.

Fluorescein angiography was performed with intravenous 10% sodium fluorescein (0.1 mL/kg). Scoring of angiograms was performed at 2 and 4 weeks post laser by a masked investigator (Supplementary Table S3). Densitometry analysis of late-stage raw angiograms was performed using ImageJ software. Because the incidence of grade IV lesions in vehicle eyes at weeks 2 and 4 was lower than the expected incidence of 25% to 40%,[40–42] an additional assessment was performed at week 6 to confirm that the laser response was not delayed.

Statistical Analyses

All data were analyzed in GraphPad and Microsoft Excel. Differences between groups or within groups were analyzed via between-group or repeated-measures ANOVA, respectively. Tukey's tests, Bonferroni tests, and *t*-tests were used for post hoc comparisons and adjusted for multiple comparisons.

Results

Vector Discovery and Characterization

Viral particles derived from a library containing approximately 10^8 variant AAV capsid sequences were administered to NHPs via IVT injection during successive rounds of in vivo competitive selection. Isolation of capsids following rounds 3 to 6 identified 5 dominant variants; each represented ≥10% of the sequenced population in a single round or ≥5% in multiple rounds (Supplementary Fig. S1). After round 6, the R100 peptide insertion sequence motif represented approximately 70% of all remaining capsid sequences (Fig. 1B). R100 was the most prevalent variant in all evaluated retinal layers, accounting for 40% to 86% of all capsid sequences in the respective layers (Fig. 1C). Sequence analysis of the R100 variant identified a 10-amino-acid peptide insertion at residue 588 in the VP3 common region and a point mutation in the VP1 region of the capsid (Fig. 1D).

Evaluation of human retinal cell transduction in vitro demonstrated efficient transduction of RPE cells, retinal ganglion cells (RGCs), and photoreceptors (Fig. 2, Supplementary Fig. S2). R100 exhibited superior transduction of

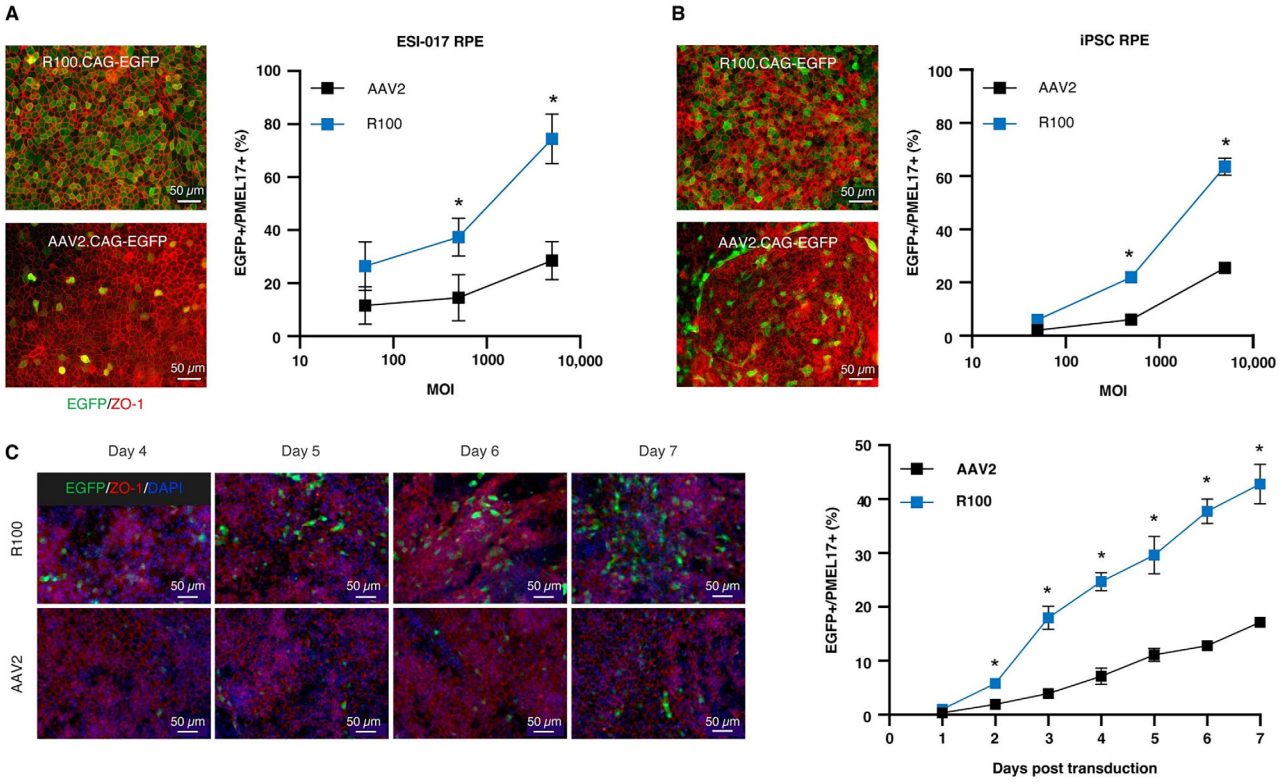

Figure 2. In vitro characterization of R100 in human RPE cells compared to AAV2. (**A, B**) Representative images and quantitation of EGFP transgene expression (*green*) 7 days post infection in **A** hESC-derived and **B** iPSC-derived RPE cells expressing ZO-1 (*red*) transduced with R100 or AAV2. Line graphs show EGFP+ cells in the PMEL17+ RPE cell population, quantified by flow cytometry. (**C**) EGFP expression kinetics following transduction by R100 or AAV2 in iPSC-derived RPE cells during the first 7 days post infection. In **C,** nuclei were counterstained with DAPI (*blue*). All images are from cultures transduced at an MOI of 5000 except for **C**, which depicts cultures transduced at an MOI of 2500. All quantitative measurements were carried out in n = 3 replicates; data are mean ± SD. *$P < 0.05$ compared to AAV2 by two-tailed *t* test. AAV, adeno-associated virus; EGFP, enhanced green fluorescent protein; hESC, human embryonic stem cell; iPSC, induced pluripotent stem cell; MOI, multiplicity of infection; RGC, retinal ganglion cell; RPE, retinal pigment epithelium.

Investigative Ophthalmology & Visual Science

both hESC-derived and iPSC-derived RPE cells compared to the wild-type AAV2 serotype (Figs. 2A, 2B). At the highest tested multiplicity of infection (MOI), 65% to 75% of the cells in R100-infected cultures were positive for EGFP expression on day 7 compared to 20% to 25% of the cells in AAV2-infected cultures (2-tailed t test, $P < 0.05$). Analysis of transgene expression kinetics showed a more rapid onset of transgene expression with R100 capsid compared to AAV2 (Fig. 2C).

Retinal transduction by R100 following IVT administration was evaluated in 2 different primate species using an EGFP reporter transgene. Administration of R100.CAG-EGFP (3×10^{11} vg/eye or 1×10^{12} vg/eye) to cynomolgus macaques resulted in time- and dose-dependent EGFP expression within the retina (Supplementary Table S1, Supplementary Fig. S3). At the 1×10^{12} vg/eye dose, widespread transduction was observed in all regions of the retina, including the fovea, macula, and periphery (Figs. 3A–I). Transgene expression was detected as early as week 1 and increased markedly by week 3. Expression increased further between weeks 3 and 8 and was stably maintained until the final assessment 6 months after administration.

The findings from in-life fundus fluorescence imaging were confirmed through post-necropsy histology assessments of EGFP immunofluorescence (see Figs. 3D–I, Supplementary Fig. S4). At the 1×10^{12} vg/eye dose, robust EGFP expression was observed in multiple retinal layers and all major cell types, including RPE cells, photoreceptors, and RGCs in the periphery, midperiphery, and macular regions (Supplementary Fig. S5).

R100-mediated retinal transduction was confirmed in a second primate species (African green monkeys) following a single IVT injection of either R100.CMV-EGFP or AAV2.CMV-EGFP (2×10^{11} vg/eye). Fundus fluorescence imaging showed retinal EGFP expression at 4, 6, 8, and 10 weeks after administration of R100 (Fig. 4). In contrast, AAV2 resulted in weak EGFP expression, which was limited to the perifoveal ring of RGCs (see Fig. 4), consistent with prior published reports.[38,43]

R100 Capsid Structure–Function Analyses

Investigation of R100 structure–function relationships through in silico modeling showed that the 10-amino-acid peptide insertion at position R588 disrupts binding to heparan sulfate, an abundant proteoglycan in the ILM.[25] Within the wild-type AAV2 capsid (the backbone for R100), amino acids R585 and R588 lie in close proximity and are precisely positioned to interact with heparan sulfate (Fig. 5A).[44,45] The peptide insertion at position R588 in R100 sterically prohibits the close proximity between R585 and R588 required for heparan sulfate binding (Fig. 5B), suggesting a plausible mechanism for enhanced transit through the heparan sulfate-rich ILM barrier. The reduced heparan sulfate binding affinity of R100 compared to AAV2 was confirmed through binding and elution from a heparin affinity column (Fig. 5C). R100 maintained dependence on the AAV receptor (AAVR) for cell transduction,[46] as demonstrated by a significant decrease in transduction of Hap1 cells lacking AAVR compared to normal Hap1 cells (Fig. 5D). Finally, the improved retinal cell transduction by R100 compared to AAV2 was associated with enhanced binding of R100 to human RPE cells (2-tailed t test, $P < 0.05$ for all comparisons; Figs. 5E, 5F).

4D-150 Transgene Expression and Activity in Human Retinal Cells

We designed 4D-150 as a recombinant dual-transgene AAV gene therapy for the treatment of wet AMD and other neovascular retinal diseases (Fig. 6A). Transduction of human RPE cells with 4D-150 resulted in dose-dependent neutralization of VEGF-A in the culture medium (Fig. 6B). Detection of excess free aflibercept protein following neutralization of VEFG-A confirmed the mechanism of action (Supplementary Fig. S6). In addition, transduction with 4D-150 led to robust expression of mature VEGF-C miRNA (Fig. 6C) and corresponding reductions in the levels of VEGF-C RNA and secreted protein compared to control (46.1% and 38.2%, respectively; Figs. 6D, 6E).

To assess the effect of 4D-150 transgene expression on human endothelial cell proliferation and migration, the 4D-150 dual payload plasmid was electroporated into VEGF-responsive HUVEC cultures. The 4D-150 plasmid cassette significantly reduced endothelial cell proliferation compared to the CAG-GFP plasmid and shock controls (1-way ANOVA, $P < 0.01$), whereas CAG-AFLB alone did not (Fig. 6F). Both the 4D-150 and CAG-AFLB plasmid cassettes reduced endothelial cell migration compared to shock control (1-way ANOVA, $P < 0.05$; Fig. 6G).

Acute Retinal Biodistribution of 4D-150 in Nonhuman Primates

Intraocular expression of 4D-150 was evaluated in cynomolgus macaques following bilateral IVT injection of 1×10^{12} vg/eye. Aqueous humor, vitreous humor, and retinal samples were analyzed for aflibercept protein and VEGF-C miRNA expression 4 weeks post administration. Secreted free aflibercept was detected in all tissue samples from all ocular compartments. Mean 4D-150 aflibercept transgene product levels were nearly 8-fold higher in the retina/choroid (mean $\pm$SD = 22,518 $\pm$ 24,981 ng aflibercept/g of tissue) compared to the aqueous humor (2,919 $\pm$ 2,366 ng aflibercept/mL). In addition, VEGF-C miRNA expression was detected (up to 91,910 copies per input RNA) from RNA isolated throughout the retina, including the superior, nasal, central, temporal, and inferior regions. RNA sequencing verified that the predominant miRNA species expressed in the primate retina after transduction with 4D-150 was the full-length targeting strand.

Efficacy of 4D-150 in a Laser-Induced CNV Model

The safety and efficacy of 4D-150 were evaluated in a laser-induced CNV study in adult male and female African green monkeys. Animals received bilateral IVT injections of either 4D-150 (1×10^{11}, 3×10^{11}, or 1×10^{12} vg/eye), R100.CAG-AFLB (1×10^{12} vg/eye), or vehicle ($n = 7$ per group).

Analysis of free aflibercept protein concentration in aqueous humor samples collected 21 days after dosing showed a dose response between the highest dose (1×10^{12} vg/eye) and the 2 lower doses (3×10^{11} and 1×10^{11} vg/eye) of 4D-150 (Fig. 7A). Of note, mean aflibercept protein concentrations were significantly higher following administration of 4D-150 1×10^{12} vg/eye compared to an equivalent dose of the single-transgene construct, R100.CAG-AFLB (2146 $\pm$ 1310 ng/mL vs. 589 $\pm$ 393 ng/mL; 1-way ANOVA with Bonferroni multiple comparisons, $P < 0.0001$; see Fig. 7A).

Investigative Ophthalmology & Visual Science

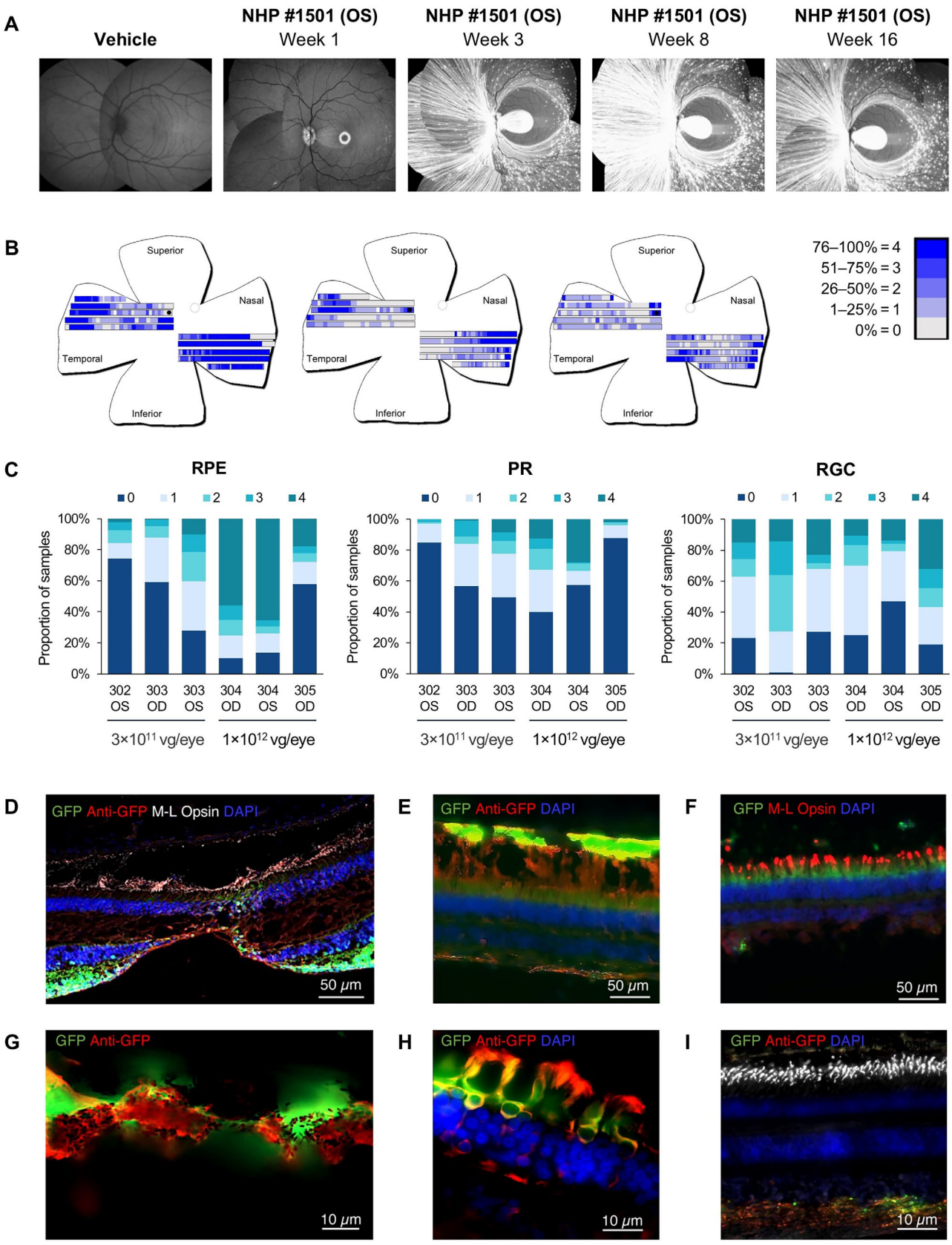

Figure 3. R100-mediated retinal transgene expression after IVT injection. All data were acquired from retinas in NHPs following administration of R100.CAG-EGFP or vehicle control. Representative fundus fluorescence images from (**A**) an eye injected with vehicle control and an eye injected with R100.CAG-EGFP 1×10^{12} vg/eye. (**B**) Representative heat map visualization of IHC scoring (NHP #304, OD). EGFP expression in the RPE layer (*left*), PR layer (*middle*), and RGC layer (*right*) was quantified for each assessed visual field and depicted as *shades of blue* corresponding to the estimated percentage of EGFP+ cells within each retinal layer. Each section was assigned a score

Investigative Ophthalmology & Visual Science

of 0 (0%), 1 (1–25%), 2 (26–50%), 3 (51–75%), or 4 (76–100%) based on the estimated proportion of cells expressing EGFP. (**C**) Assessment of EGFP expression in NHP eye sections by IHC 8 weeks after administration of R100.CAG-EGFP 3×10^{11} vg/eye or 1×10^{12} vg/eye. (**D**) Representative image of transduced cells in the central retina showing robust EGFP expression in foveal cone PRs (*white*) and RGCs. (**E, F**) Representative images demonstrating robust EGFP expression in peripheral PRs **E** and co-localized with opsin (*red*) **F**. (**G–I**) Representative images of EGFP expression in RPE **G**, the outer segments of PR **H**, and the axons of RGCs **I**. EGFP expression (*green*) is also detected by an anti-GFP antibody (red) in all images except **F**. Nuclei were counterstained with DAPI (*blue*) except in **G**. EGFP, enhanced green fluorescent protein; IHC, immunohistochemistry; IVT, intravitreal injection; NHP, nonhuman primate; PR, photoreceptor; RGC, retinal ganglion cell; RPE, retinal pigment epithelium.

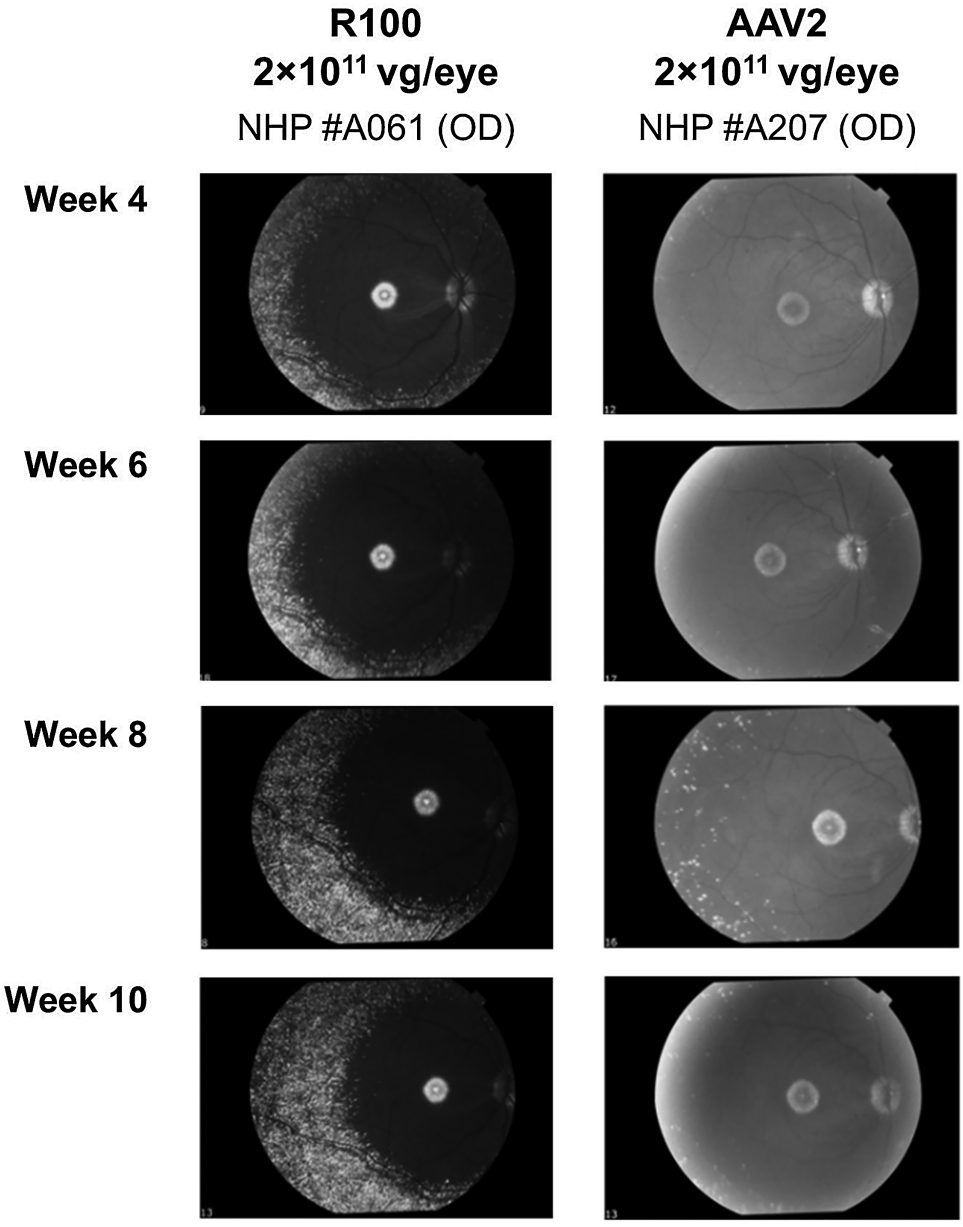

Figure 4. Widespread transduction of the NHP retina after IVT administration of R100 compared to AAV2. Data were acquired from retinas in African green monkeys 4 to 10 weeks post administration of 2×10^{11} vg/eye of R100.CMV-EGFP or AAV2.CMV-EGFP ($N = 3$ animals and $N = 4$ eyes per group). All animals were seronegative for pre-existing neutralizing antibodies to the R100 and AAV2 capsids. The lower exposure setting in the R100 images was necessary to compensate for the strength of the GFP signal; formal quantification of the GFP signal was not feasible. AAV, adeno-associated virus; IVT, intravitreal injection; NHP, nonhuman primate.

The in vivo efficacy of 4D-150 was evaluated in the laser-induced CNV model based on the incidence of grade IV lesions and the CNV fibrovascular complex area (determined by the cross-sectional area of hyper-reflective formation at the principal axis on optical coherence tomography [OCT]). At 2 weeks post laser administration, a significant reduction in the incidence of grade IV CNV lesions was observed at all tested doses of 4D-150 compared to vehicle (Fisher's Exact Prob test, $P < 0.005$ for all comparisons). No grade IV lesions were observed in any 4D-150–treated animals at

Investigative Ophthalmology & Visual Science

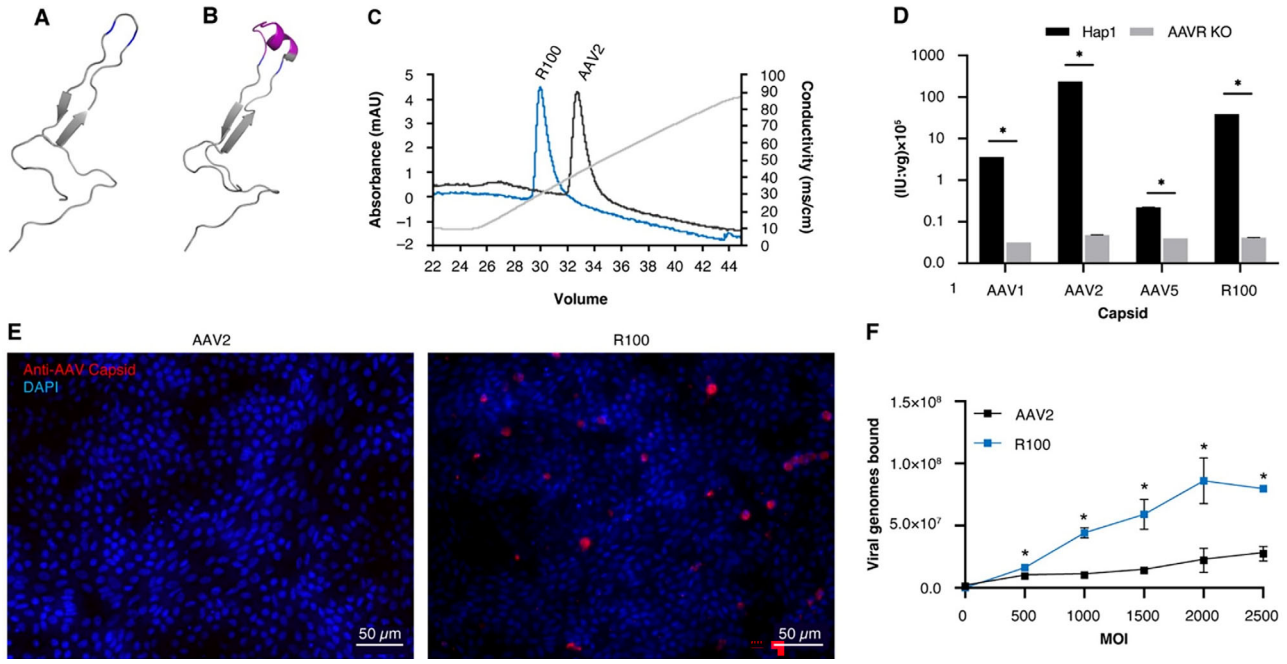

Figure 5. Structure–function analysis demonstrating a disruption of the heparan sulfate binding domain in R100 through a 10-amino-acid peptide insertion in the GH loop and an increase in retinal cell binding. Molecular models of the GH loop within the VP3 common region of (**A**) AAV2 and (**B**) R100. The R100 peptide sequence (*magenta*) is constrained by the location of amino acids R585 and R588 (*blue*) within the intact capsid. (**C**) AAV2 and R100 vectors bound to and eluted from a heparin affinity column. R100 capsid elutes at a lower conductivity compared to AAV2, demonstrating a decrease in heparin affinity. (**D**) AAV vectors were used to transduce Hap1 and AAVR KO Hap1 cell lines. All vectors demonstrate a cell surface receptor dependence on AAVR. $N = 3$ replicates each. *$P < 0.05$ by paired t test between Hap1 and AAVR KO within each serotype. (**E**) Representative images of AAV2 and R100 binding to human iPSC-derived RPE (MOI = 2500), visualized using an anti-AAV2 capsid antibody (*red*). **(F)** The number of AAV2 and R100 viral genomes bound to human iPSC-derived RPE was quantified across a range of MOIs. Error bars indicate standard deviation. *$P < 0.05$ by two-tailed t test. AAV, adeno-associated virus; AAVR, AAV receptor; iPSC, induced pluripotent stem cell; KO, knockout; MOI, multiplicity of infection; RPE, retinal pigment epithelium.

week 2 or at any subsequent time point (Fig. 7B, Supplementary Table S4). By comparison, grade IV lesions were observed in 1.2% and 12% of animals in the R100.CAG-AFLB and vehicle-treated groups, respectively, at week 2 (Fisher's Exact Prob test, $P < 0.01$). The CNV complex area was significantly smaller in the 4D-150–treated groups compared to the vehicle group (52%–62% reduction; 2-way ANOVA followed by Tukey-Kramer Honestly Significant Difference (HSD), $P < 0.005$ for all comparisons; Fig. 7C). The lowest tested dose of 4D-150 (1×10^{11} vg/eye) conferred equivalent protection against CNV compared to the highest dose (1×10^{12} vg/eye).

Safety and Tolerability of 4D-150

In-life eye assessments performed prior to laser photocoagulation in NHPs demonstrated that 4D-150 was generally well tolerated. At week 6, immediately prior to induction of CNV, there was no evidence of any of the following toxicities: aqueous flare, vitreous haze, lens capsule deposit/lens opacity, fibrin strands, iris/ciliary body (hyperemia, exfoliation, or synechia), conjunctival (congestion, swelling, or discharge), corneal (vascularization, opacity, or opacity area), hypopyon, retinal vasculitis, or papillitis. In addition, there were no adverse effects on retinal morphology, vascular integrity, or on the optic nerve head (Supplementary Fig. S7). Inflammation was generally absent or mild (Supplementary Fig. S8). A dose response was observed for white blood cells in the aqueous and vitreous humor. At 1×10^{11} vg/eye, no inflammation was observed in any eyes (0/14) in either the aqueous or vitreous humor. At 3×10^{11} vg/eye, 3 of 14 (21%) eyes had inflammation in aqueous humor (2 eyes $\geq$ grade 2) and 4 of 14 (29%) had inflammation in the vitreous humor (2 eyes $\geq$ grade 2). At 1×10^{12} vg/eye, 7 of 14 (50%) eyes had inflammation in aqueous humor (3 eyes $\geq$ grade 2) and 2 of 14 (14%) had inflammation in the vitreous humor (1 eye, grade 2).

Serum aflibercept concentrations were below the lower limit of quantitation in all animals and at all time points in the 1×10^{11} vg/eye dose group. Low concentrations of aflibercept were detected in serum in 2 of 7 animals in both the 3×10^{11} and 1×10^{12} vg/eye dose groups; of these, only one animal in the 3×10^{11} vg/eye treatment group had quantifiable levels at more than one time point (Supplementary Table S5).

OCT-derived retinal volume and retinal thickness showed no evidence of retinal edema or degeneration-related thinning during the 22-week observation period (Supplementary Fig. S9A). Full-field electroretinography was conducted at weeks 12 and 22 to screen for adverse effects on retinal function over time. No statistically significant difference was observed between groups in scotopic a-wave, scotopic b-wave, or photopic flicker, and no significant differences were observed between different time points (Supplementary Fig. S9B). Hypotony was not observed in any 4D-150–treated eyes (Supplementary Fig. S9C). Postmortem analysis performed at 22 weeks revealed no adverse findings in ocular tissue, including the iris, ciliary body, and retina, in any animal in any dose group.

Investigative Ophthalmology & Visual Science

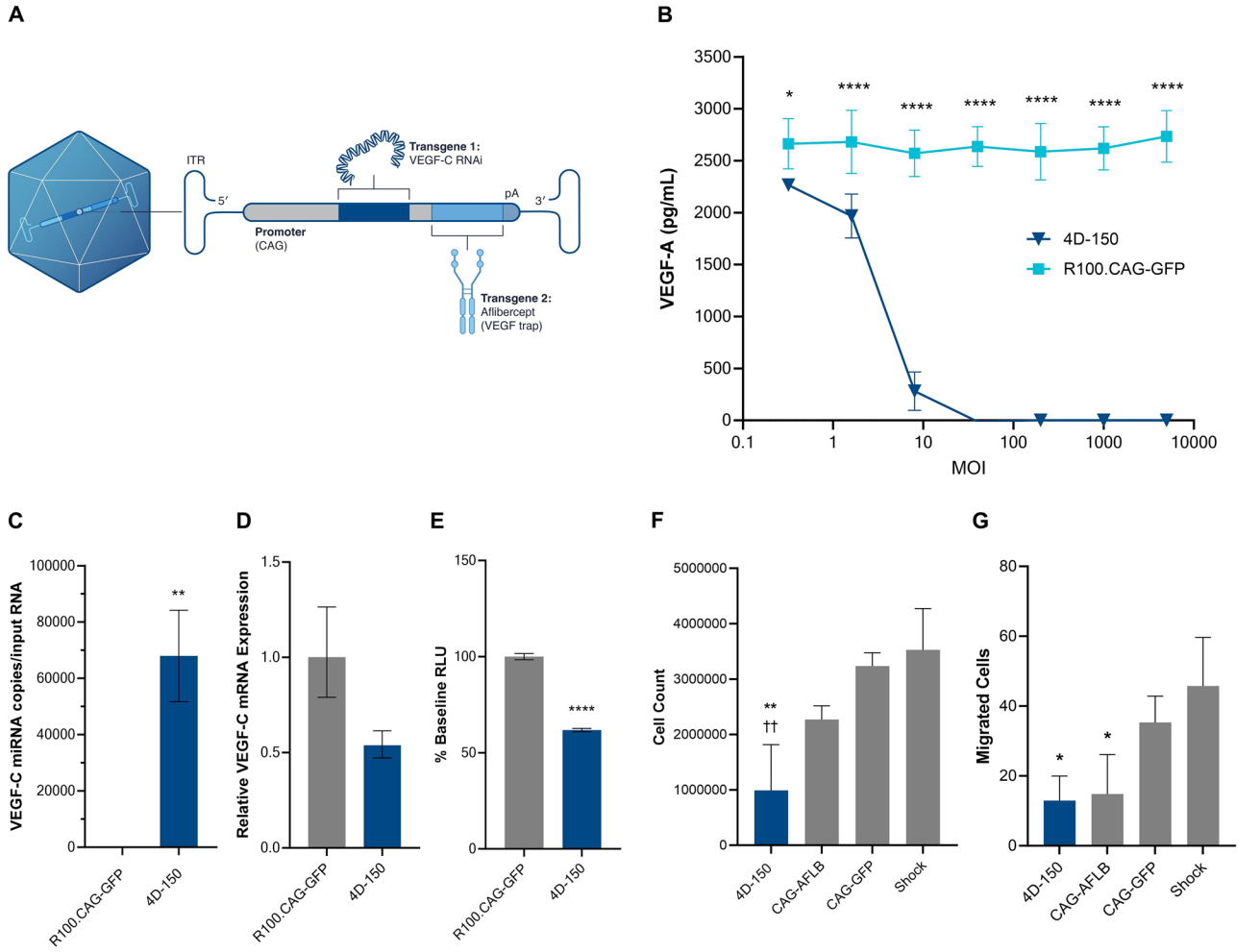

Figure 6. The 4D-150 dual-transgene expression and function in vitro. (**A**) Schema of 4D-150, a dual-transgene anti-angiogenic AAV gene therapy product. (**B**) Analysis of VEGF-A protein neutralization in the medium of human RPE transduced with 4D-150 or control R100.CAG-GFP vector, data are mean ± SD, $^{*}P < 0.05$, $^{****}P < 0.0001$ by 2-way ANOVA with Tukey's multiple comparison post hoc test. (**C**) Expression of mature anti-VEGF-C miRNA measured by quantitative reverse transcription PCR (RT-qPCR) from transduced human RPE (MOI = 1000) in response to 4D-150 treatment, data are mean ± SD, $^{**}P < 0.005$ by unpaired *t* test. (**D**) RT-qPCR analysis of VEGF-C transcript levels in transduced RPE (MOI = 1000), normalized to Ribosomal Protein L32 as the housekeeping control. Mean ±SD. (**E**) Analysis of secreted VEGF-C protein from transduced RPE (MOI = 1000). BLQ values are represented as "0", data are mean ± SD. $^{****}P < 0.0001$ by unpaired *t* test. Analysis of (**F**) proliferation and (**G**) migration of HUVEC cultures in a Transwell system after electroporation with the respective plasmid construct ($N = 3$, data are mean ± SD. $^{**}P < 0.01$ compared to shock (electroporation control), $^{*}P < 0.05$ compared to shock, $^{\dagger\dagger}P < 0.01$ compared to CAG-GFP by 1-way ANOVA with Tukey's multiple comparison post hoc test. AFLB, aflibercept; BLQ, below the limit of quantification; GFP, green fluorescent protein; HUVEC, human umbilical vein endothelial cells; ITR, inverted terminal repeats; MOI, multiplicity of infection; RLU, relative luciferase units; RPE, retinal pigment epithelium; VEGF, vascular endothelial growth factor.

Discussion

Targeted retinal delivery of therapeutic transgenes encoding recombinant proteins and/or RNAi molecules offers the potential to provide durable and consistent suppression of pathological ocular angiogenesis, thus reducing the treatment burden and potentially improving long-term vision outcomes for patients with diseases such as wet AMD and DME. Retinal gene therapies employing wild-type AAV vectors have demonstrated the potential for therapeutic efficacy in wet AMD[47–49]; however, the limited capacity of wild-type AAV serotypes to penetrate vitreoretinal barriers after IVT injection remains a persistent challenge.Novel AAV vectors are therefore needed for IVT delivery of transgenes to the retina in humans.

To address the limited retinal transduction capacity of wild-type AAV vectors after IVT injection, we used directed evolution in NHPs to invent a retinotropic AAV capsid (R100) that exhibits widespread transduction of all major retinal cell types following IVT injection. In vitro studies evaluating R100 demonstrated superior transduction of human retinal cells compared to AAV2. In NHPs, IVT administration of R100 resulted in widespread transduction of all major retinal cell types and all retinal cell layers. In marked contrast to AAV2, robust EGFP expression was observed in the central, mid-peripheral, and peripheral regions of the retina. Structure–function analyses demonstrated that the 10-amino-acid peptide insertion at position R588 in the R100 capsid reduces heparin binding affinity and facilitates transit through the heparan sulfate-rich ILM, suggesting a putative mechanism for enhanced delivery to cells within the retina. The precise mechanism through which the observed improvement in retinal cell binding and entry compared to wild-type AAV2 is mediated has not yet been elucidated;

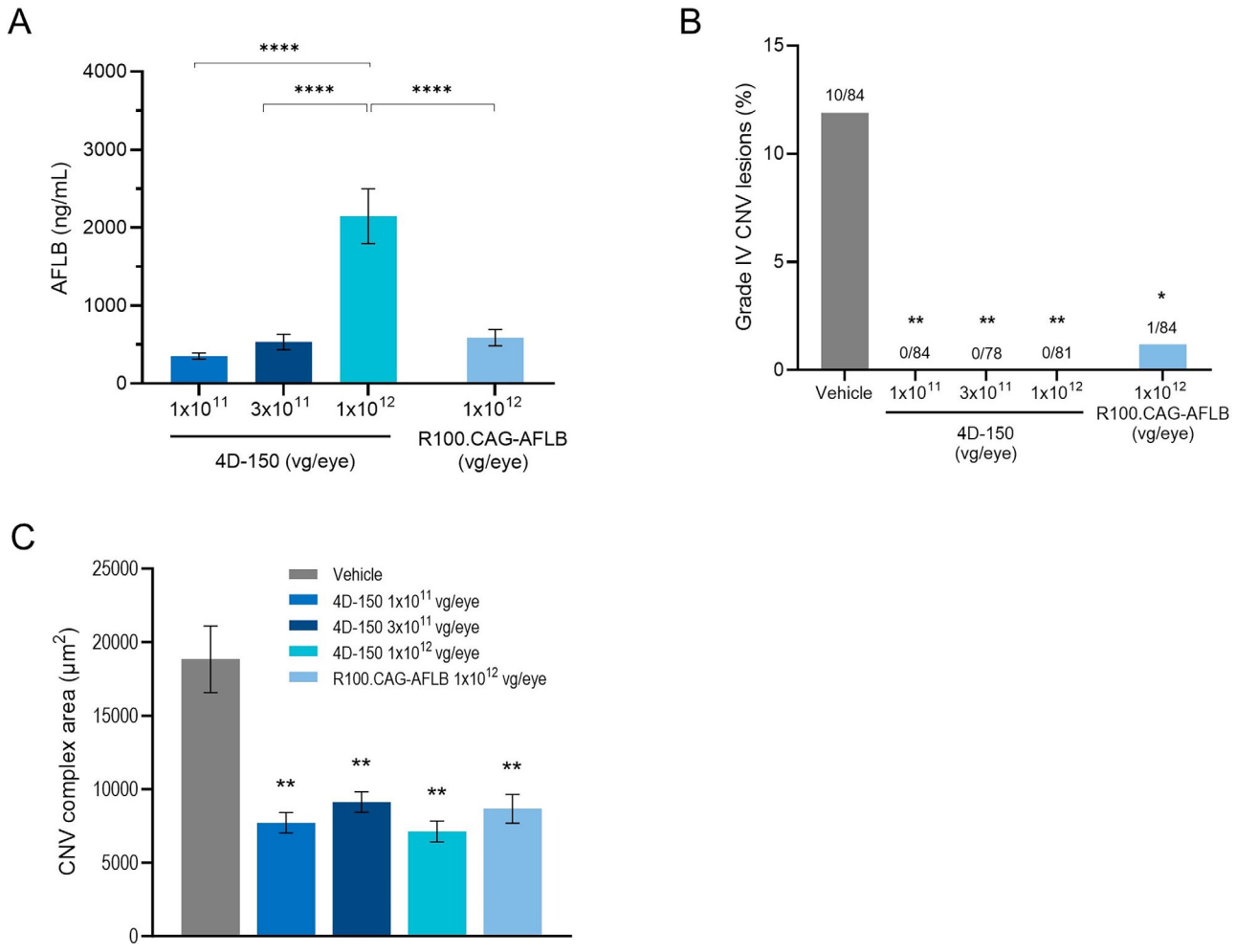

Figure 7. Aflibercept protein expression and laser-induced CNV lesions in primates following IVT administration of 4D-150 or control. **(A)** Secreted free aflibercept protein expression in the aqueous humor by treatment group 21 days post IVT administration ($n = 14$ eyes per group) and prior to laser-induced CNV, data are mean ± SD. ****$P < 0.0001$ by 1-way ANOVA with Bonferroni's multiple comparisons. **(B)** Percentage of eyes with grade IV lesions 2 weeks post laser per treatment group. **$P < 0.005$, *$P < 0.01$ compared to vehicle by Fisher's Exact Prob test. **(C)** Reduced CNV complex area with 4D-150 pretreatment at 4 weeks post laser. Data are mean ± SEM. CNV complex areas of the principal axis of each lesion were calculated for each treatment group. Pretreatment with all doses of 4D-150 resulted in significantly smaller mean CNV complex areas compared to vehicle. **$P < 0.005$ by 2-way ANOVA followed by Tukey-Kramer HSD. AFLB, aflibercept; CNV, choroidal neovascularization; IVT, intravitreal.

investigation of R100 binding to known AAV glycan co-receptors and potentially other unidentified receptors will be the subject of future work.

The R100-based gene therapy 4D-150 was engineered to provide durable suppression of angiogenic signaling pathways in the retina through sustained expression of 2 therapeutic transgenes targeting 4 different members of the VEGF family. The design of the dual-transgene cassette was supported by several lines of evidence. Numerous animal studies have demonstrated that overexpression and secretion of VEGF from the RPE induces CNV.[50–54] Concentrations of VEGF-A, VEGF-B, and PlGF are elevated in the eyes of individuals with wet AMD compared to healthy controls,[21,54,55] and VEGF-C is highly expressed in RPE cells in human choroidal neovascular membranes.[56] VEGF-A, VEGF-B, and PlGF promote angiogenesis via binding interactions with VEGFR1 and/or VEGFR2. VEGF-C signals through VEGFR2 and VEGFR3 to promote proliferation and migration of endothelial cells to form lymphatic and angiogenic vessels,[22] and has been shown to promote vessel permeability and vascular leakage.[23] In addition, VEGF-C concentrations are reportedly elevated in the eye following treatment with VEGF-A inhibitors, suggesting that VEGF-A suppression induces compensatory upregulation of VEGF-C.[21,23,24] In a randomized phase II clinical trial in patients with wet AMD, combined administration of a monoclonal antibody targeting VEGF-C/-D and the anti-VEGF-A antibody ranibizumab was superior to ranibizumab alone.[57]

Consistent with the design characteristics of the dual-transgene payload, transduction of human RPE cells with 4D-150 led to dose-dependent neutralization of VEGF-A and a marked reduction in VEGF-C expression. IVT administration of 4D-150 to NHPs was safe and generally well tolerated and resulted in robust retinal transgene expression. In addition, 4D-150 completely suppressed grade IV angiogenic lesions in a primate model of laser-induced CNV. Notably, the lowest tested dose (1×10^{11} vg/eye) conferred equal protection against CNV compared to the highest tested dose (1×10^{12} vg/eye), suggesting that lower doses are likely to be clinically active.

Our findings should be interpreted in the context of the limitations of in vitro and NHP models, which do not fully recapitulate the complex interactions between human ocular pathology, viral transduction dynamics, and immune response. We selected NHPs for in vivo directed evolution of AAV capsids based in part on key structural similarities between NHP and human eyes, including ILM thickness and overall volume,[58] as well as similarities between NHP and human immune systems. Despite these similarities, the degree to which the findings from preclinical models are translatable to humans is uncertain. We note, however, that interim results from an ongoing phase I/II clinical trial (PRISM) evaluating 4D-150 in individuals with wet AMD were consistent with observations from NHP studies (Khanani AM, et al. *IOVS* 2023;64:ARVO E-Abstract 5055).[59,60] Intravitreal administration of 4D-150 was well tolerated, with no serious adverse events and no clinically significant inflammation or hypotony during follow up for 24 to 36 weeks. Evaluation of biological activity showed evidence of stabilization in central subfield thickness and a reduction in the frequency of anti-VEGF injections, including an 89% reduction in the mean annualized injection rate at 24 weeks in the 3×10^{10} vg/eye group in the phase II dose expansion cohort ($n = 20$). Consistent with prior evidence,[61] the primate CNV model used to evaluate the efficacy of 4D-150 in vivo was highly responsive to aflibercept alone, precluding evaluation of the potential incremental anti-angiogenic benefit of the VEGF-C RNAi transgene, although evidence of an incremental antiproliferative effect was observed in a human endothelial cell model in vitro. Interestingly, IVT administration of 4D-150 to NHPs resulted in significantly higher levels of aflibercept protein in aqueous humor samples compared to an equivalent dose of the single-transgene construct (R100.CAG-AFLB), suggesting that the VEGF-C RNAi transgene or its position within the transgene cassette promotes aflibercept expression. Further research is required to evaluate the therapeutic benefit of the VEGF-C RNAi transgene and elucidate the mechanism(s) related to the observed increase in aflibercept transgene expression.

In summary, 4D-150 resulted in efficient expression and function of both anti-angiogenic transgenes in human retinal and vascular endothelial cells in vitro. IVT administration of 4D-150 to NHPs was well tolerated and led to robust retinal transgene expression and clinical activity. These findings support continued evaluation of 4D-150 as a potential therapy for neovascular retinal diseases. Clinical trials are underway to establish the safety and efficacy of 4D-150 in individuals with wet AMD (NCT05197270) and DME (NCT05930561).

Acknowledgments

The authors thank Robert Kim, An Song, and Kenneth Glasscock for review of the manuscript and to David Suhy for oversight and management of the African green monkey R100-GFP study. They also thank Charles River Laboratories, Valley Biosystems, and Virscio, Inc., for technical assistance with the in vivo studies.

Supported by 4D Molecular Therapeutics.

Medical writing, editing, and publication assistance were provided by Scient Healthcare Communications.

Author Contributions: M.A.C., R.H.C., C.B., T.V., M.L., J.H., G.B., M.K., D.S., P.F., and D.K. conceived and designed the experiments. R.H.C., C.B., T.V., P.S., C.S., A.K., M.Q., and M.H. performed the experiments. M.A.C., R.H.C., C.B., T.V., P.S., C.S., A.K., M.L., M.Q., A.M.K., and M.H. analyzed the data. K.B., D.K., T.M., and K.D. contributed materials/analysis tools. M.A.C., R.H.C., P.F., and D.K. wrote the paper.

Disclosure: **M.A. Calton**, 4DMT (E, I) and is an inventor on the following relevant international patent filings assigned to 4DMT (P): PCT/US2022/026395; **R.H. Croze**, 4DMT (E, I); **C. Burns**, 4DMT, (I); and former employee at 4DMT, and is an inventor on the following relevant international patent filings assigned to 4DMT (P): PCT/US2022/026395; **G. Beliakoff** None; **T. Vazin**, 4DMT (I) and former employee at 4DMT; **P. Szymanksi,** 4DMT, (I); and former employee at 4DMT and is an inventor on the following relevant international patent filings assigned to 4DMT (P): PCT/US2022/026395 and WO2019104279A1; **C. Schmitt**, former employee at 4DMT, has unvested stock options and is a current employee at Codexis Inc. (E, I); **A. Klein**, 4DMT (I) and former employee at 4DMT; **M. Leong**, 4DMT, (P, I) and former employee at 4DMT; **M. Quezada**, 4DMT (E, I); **J. Holt**, 4DMT (I) and former employee at 4DMT; **G. Bolender**, 4DMT (I) and former employee at 4DMT; **K. Barglow**, 4DMT (E, I); **D. Khoday**, 4DMT (E, I); **T. Mason**, 4DMT (E, I); **K. Delaria**, 4DMT (E, I); **M. Hassanipour,** is a former employee at 4DMT (I); **M. Kotterman**, former employee at 4DMT (I), and is an inventor on the following relevant international patent filings assigned to 4DMT (P): WO2017197355A2 and WO2019104279A1; **A.M. Khanani**, has served as a consultant to and/or received research support from 4DMT (C, F), AbbVie (C, F), Adverum (C, F), Alcon (C, F), Alexion (C, F), Amgen (C, F), Annexin (C, F), Annexon (C, F), Apellis Pharmaceuticals (C, F), Aviceda Therapeutics (C, F), Beacon Therapeutics (C, F), Clearside Biomedical (C, F), Complement Therapeutics (C, F), Exegenesis (C, F), EyePoint Pharmaceuticals (C, F), Fronterra Therapeutics (C, F), Genentech (C, F), Gyroscope Therapeutics (C, F), i-Lumen Scientific (C, F), Iveric Bio (C, F), Janssen Pharmaceuticals (C, F), Kodiak Sciences (C, F), Kriya Therapeutics (C, F), Nanoscope (C, F), Neurotech (C, F), Novartis (C, F), Ocular Therapeutix (C, F), Oculis (C, F), Ocuphire (C, F), OcuTerra (C, F), Olive BioPharma (C, F), Opthea (C, F), Oxular (C, F), Oxurion (C, F), Perfuse (C, F), Ray Therapeutics (C, F), Recens Medical (C, F), Regeneron Pharmaceuticals (C, F), Regenxbio (C, F), Revive (C, F), RevOpsis (C, F), Roche (C, F), Sanofi (C, F), Stealth BioTherapeutics (C, F), Thea Pharma (C, F), Unity Biotechnology (C, F), Vanotech (C, F), Vial (C, F), and Unity Biotechnology (C, F); Aviceda Therapeutics (I), Oculis (I), PolyPhotonix (I), Recens Medical (I), Perfuse (I), RevOpsis (I), and Vial (I); **D. Schaffer**, 4DMT (C, I), has received sponsored research funding from 4DMT (F), and is an inventor on the following relevant international patent filings assigned to 4DMT (P): WO2017197355A2 and WO2019104279A1; **P. Francis**, former employee at 4DMT (I), and is an inventor on the following relevant international patent filing assigned to 4DMT (P): WO2019104279A1; **D. Kirn**, is the chief executive officer at 4DMT with salary, bonus, stock and stock options, and is an inventor on the following relevant international patent filings assigned to 4DMT (P): WO2017197355A2 and WO2019104279A1

References

1. Jonas JB, Cheung CMG, Panda-Jonas S. Updates on the epidemiology of age-related macular degeneration. *Asia Pac J Ophthalmol (Phila)*. 2017;6:493–497.
2. Wong WL, Su X, Li X, et al. Global prevalence of age-related macular degeneration and disease burden projection for 2020 and 2040: a systematic review and meta-analysis. *Lancet Glob Health*. 2014;2:e106–e116.
3. Hobbs SD, Pierce K. Wet age-related macular degeneration (Wet AMD). *StatPearls*. Treasure Island (FL): StatPearls Publishing; 2022.
4. Spaide RF, Jaffe GJ, Sarraf D, et al. Consensus nomenclature for reporting neovascular age-related macular degen-

eration data: consensus on neovascular age-related macular degeneration nomenclature study group. *Ophthalmology.* 2020;127:616–636.
5. Amoaku WM, Ghanchi F, Bailey C, et al. Diabetic retinopathy and diabetic macular oedema pathways and management: UK Consensus Working Group. *Eye (Lond).* 2020;34:1–51.
6. Amoaku WM, Ghanchi F, Bailey C, et al. Correction: Diabetic retinopathy and diabetic macular oedema pathways and management: UK Consensus Working Group. *Eye (Lond).* 2020;34:1941–1942.
7. Bakri SJ, Thorne JE, Ho AC, et al. Safety and efficacy of anti-vascular endothelial growth factor therapies for neovascular age-related macular degeneration: a report by the American Academy of Ophthalmology. *Ophthalmology.* 2019;126:55–63.
8. Brown D, Heier JS, Boyer DS, et al. Current best clinical practices—management of neovascular AMD. *J Vitreoretin Dis.* 2017;1:294–297.
9. Fauser S, Schwabecker V, Muether PS. Suppression of intraocular vascular endothelial growth factor during aflibercept treatment of age-related macular degeneration. *Am J Ophthalmol.* 2014;158:532–536.
10. Gragoudas ES, Adamis AP, Cunningham ET, Jr., Feinsod M, Guyer DR, VEGF Inhibition Study in Ocular Neovascularization Clinical Trial Group. Pegaptanib for neovascular age-related macular degeneration. *N Engl J Med.* 2004;351:2805–2816.
11. Comparison of Age-related Macular Degeneration Treatments Trials Research G, Martin DF, Maguire MG, et al. Ranibizumab and bevacizumab for neovascular age-related macular degeneration. *N Engl J Med.* 2011;364:1897–1908.
12. Lotery A, Griner R, Ferreira A, Milnes F, Dugel P. Real-world visual acuity outcomes between ranibizumab and aflibercept in treatment of neovascular AMD in a large US data set. *Eye (Lond).* 2017;31:1697–1706.
13. Rosenfeld PJ, Brown DM, Heier JS, et al. Ranibizumab for neovascular age-related macular degeneration. *N Engl J Med.* 2006;355:1419–1431.
14. Al-Khersan H, Hussain RM, Ciulla TA, Dugel PU. Innovative therapies for neovascular age-related macular degeneration. *Expert Opin Pharmacother.* 2019;20:1879–1891.
15. Brown DM, Kaiser PK, Michels M, et al. Ranibizumab versus verteporfin for neovascular age-related macular degeneration. *N Engl J Med.* 2006;355:1432–1444.
16. Heier JS, Brown DM, Chong V, et al. Intravitreal aflibercept (VEGF trap-eye) in wet age-related macular degeneration. *Ophthalmology.* 2012;119:2537–2548.
17. Almuhtaseb H, Johnston RL, Talks JS, Lotery AJ. Second-year visual acuity outcomes of nAMD patients treated with aflibercept: data analysis from the UK aflibercept users group. *Eye (Lond).* 2017;31:1582–1588.
18. Ciulla TA, Huang F, Westby K, Williams DF, Zaveri S, Patel SC. Real-world outcomes of anti-vascular endothelial growth factor therapy in neovascular age-related macular degeneration in the United States. *Ophthalmol Retina.* 2018;2:645–653.
19. Comparison of Age-related Macular Degeneration Treatments Trials Research G, Maguire MG, Martin DF, et al. Five-year outcomes with anti-vascular endothelial growth factor treatment of neovascular age-related macular degeneration: the comparison of age-related macular degeneration treatments trials. *Ophthalmology.* 2016;123:1751–1761.
20. Khanani AM, Skelly A, Bezlyak V, Griner R, Torres LR, Sagkriotis A. SIERRA-AMD: a retrospective, real-world evidence study of patients with neovascular age-related macular degeneration in the United States. *Ophthalmol Retina.* 2020;4:122–133.
21. Cabral T, Lima LH, Mello LGM, et al. Bevacizumab injection in patients with neovascular age-related macular degeneration increases angiogenic biomarkers. *Ophthalmol Retina.* 2018;2:31–37.
22. Hsu MC, Pan MR, Hung WC. Two birds, one stone: double hits on tumor growth and lymphangiogenesis by targeting vascular endothelial growth factor receptor 3. *Cells.* 2019;8:270.
23. Cao R, Eriksson A, Kubo H, Alitalo K, Cao Y, Thyberg J. Comparative evaluation of FGF-2-, VEGF-A-, and VEGF-C-induced angiogenesis, lymphangiogenesis, vascular fenestrations, and permeability. *Circ Res.* 2004;94:664–670.
24. Pongsachareonnont P, Mak MYK, Hurst CP, Lam WC. Neovascular age-related macular degeneration: intraocular inflammatory cytokines in the poor responder to ranibizumab treatment. *Clin Ophthalmol.* 2018;12:1877–1885.
25. Dalkara D, Kolstad KD, Caporale N, et al. Inner limiting membrane barriers to AAV-mediated retinal transduction from the vitreous. *Mol Ther.* 2009;17:2096–2102.
26. Jacobson SG, Cideciyan AV, Ratnakaram R, et al. Gene therapy for Leber congenital amaurosis caused by RPE65 mutations: safety and efficacy in 15 children and adults followed up to 3 years. *Arch Ophthalmol.* 2012;130:9–24.
27. MacLaren RE, Groppe M, Barnard AR, et al. Retinal gene therapy in patients with choroideremia: initial findings from a phase 1/2 clinical trial. *Lancet.* 2014;383:1129–1137.
28. Asuri P, Bartel MA, Vazin T, Jang JH, Wong TB, Schaffer DV. Directed evolution of adeno-associated virus for enhanced gene delivery and gene targeting in human pluripotent stem cells. *Mol Ther.* 2012;20:329–338.
29. Jang JH, Koerber JT, Kim JS, et al. An evolved adeno-associated viral variant enhances gene delivery and gene targeting in neural stem cells. *Mol Ther.* 2011;19:667–675.
30. Koerber JT, Jang JH, Schaffer DV. DNA shuffling of adeno-associated virus yields functionally diverse viral progeny. *Mol Ther.* 2008;16:1703–1709.
31. Koerber JT, Jang JH, Yu JH, Kane RS, Schaffer DV. Engineering adeno-associated virus for one-step purification via immobilized metal affinity chromatography. *Hum Gene Ther.* 2007;18:367–378.
32. Koerber JT, Klimczak R, Jang JH, Dalkara D, Flannery JG, Schaffer DV. Molecular evolution of adeno-associated virus for enhanced glial gene delivery. *Mol Ther.* 2009;17:2088–2095.
33. Koerber JT, Maheshri N, Kaspar BK, Schaffer DV. Construction of diverse adeno-associated viral libraries for directed evolution of enhanced gene delivery vehicles. *Nat Protoc.* 2006;1:701–706.
34. Maheshri N, Koerber JT, Kaspar BK, Schaffer DV. Directed evolution of adeno-associated virus yields enhanced gene delivery vectors. *Nat Biotechnol.* 2006;24:198–204.
35. Marsic D, Govindasamy L, Currlin S, et al. Vector design Tour de Force: integrating combinatorial and rational approaches to derive novel adeno-associated virus variants. *Mol Ther.* 2014;22:1900–1909.
36. Dalkara D, Byrne LC, Klimczak RR, et al. In vivo-directed evolution of a new adeno-associated virus for therapeutic outer retinal gene delivery from the vitreous. *Sci Transl Med.* 2013;5:189ra176.
37. Ye GJ, Budzynski E, Sonnentag P, et al. Safety and biodistribution evaluation in cynomolgus macaques of rAAV2tYF-CB-hRS1, a recombinant adeno-associated virus vector expressing retinoschisin. *Hum Gene Ther Clin Dev.* 2015;26:165–176.

38. Yin L, Greenberg K, Hunter JJ, et al. Intravitreal injection of AAV2 transduces macaque inner retina. *Invest Ophthalmol Vis Sci.* 2011;52:2775–2783.
39. Yin L, Masella B, Dalkara D, et al. Imaging light responses of foveal ganglion cells in the living macaque eye. *J Neurosci.* 2014;34:6596–6605.
40. Goody RJ, Hu W, Shafiee A, et al. Optimization of laser-induced choroidal neovascularization in African green monkeys. *Exp Eye Res.* 2011;92:464–472.
41. Grishanin R, Vuillemenot B, Sharma P, et al. Preclinical evaluation of ADVM-022, a novel gene therapy approach to treating wet age-related macular degeneration. *Mol Ther.* 2019;27:118–129.
42. Sidman RL, Li J, Lawrence M, et al. The peptidomimetic Vasotide targets two retinal VEGF receptors and reduces pathological angiogenesis in murine and nonhuman primate models of retinal disease. *Sci Transl Med.* 2015;7:309ra165.
43. Boye SE, Alexander JJ, Witherspoon CD, et al. Highly efficient delivery of adeno-associated viral vectors to the primate retina. *Hum Gene Ther.* 2016;27:580–597.
44. Kern A, Schmidt K, Leder C, et al. Identification of a heparin-binding motif on adeno-associated virus type 2 capsids. *J Virol.* 2003;77:11072–11081.
45. Opie SR, Warrington KH, Jr., Agbandje-McKenna M, Zolotukhin S, Muzyczka N. Identification of amino acid residues in the capsid proteins of adeno-associated virus type 2 that contribute to heparan sulfate proteoglycan binding. *J Virol.* 2003;77:6995–7006.
46. Pillay S, Meyer NL, Puschnik AS, et al. An essential receptor for adeno-associated virus infection. *Nature.* 2016;530:108–112.
47. Constable IJ, Pierce CM, Lai CM, et al. Phase 2a randomized clinical trial: safety and post hoc analysis of subretinal rAAV.sFLT-1 for wet age-related macular degeneration. *EBioMedicine.* 2016;14:168–175.
48. Rakoczy EP, Lai CM, Magno AL, et al. Gene therapy with recombinant adeno-associated vectors for neovascular age-related macular degeneration: 1 year follow-up of a phase 1 randomised clinical trial. *Lancet.* 2015;386:2395–2403.
49. Liu Y, Fortmann SD, Shen J, et al. AAV8-antiVEGFfab ocular gene transfer for neovascular age-related macular degeneration. *Mol Ther.* 2018;26:542–549.
50. Cui JZ, Kimura H, Spee C, Thumann G, Hinton DR, Ryan SJ. Natural history of choroidal neovascularization induced by vascular endothelial growth factor in the primate. *Graefes Arch Clin Exp Ophthalmol.* 2000;238:326–333.
51. Grossniklaus HE, Kang SJ, Berglin L. Animal models of choroidal and retinal neovascularization. *Prog Retin Eye Res.* 2010;29:500–519.
52. Pennesi ME, Neuringer M, Courtney RJ. Animal models of age related macular degeneration. *Mol Aspects Med.* 2012;33:487–509.
53. Vinores SA, Xiao WH, Aslam S, et al. Implication of the hypoxia response element of the Vegf promoter in mouse models of retinal and choroidal neovascularization, but not retinal vascular development. *J Cell Physiol.* 2006;206:749–758.
54. Shahidatul-Adha M, Zunaina E, Aini-Amalina MN. Evaluation of vascular endothelial growth factor (VEGF) level in the tears and serum of age-related macular degeneration patients. *Sci Rep.* 2022;12:4423.
55. Sharma K, Sharma NK, Singh R, Anand A. Exploring the role of VEGF in Indian age-related macular degeneration. *Ann Neurosci.* 2015;22:232–237.
56. Otani A, Takagi H, Oh H, et al. Vascular endothelial growth factor family and receptor expression in human choroidal neovascular membranes. *Microvasc Res.* 2002;64:162–169.
57. Jackson TL, Slakter J, Buyse M, et al. A randomized controlled trial of OPT-302, a VEGF-C/D inhibitor for neovascular age-related macular degeneration. *Ophthalmology.* 2023;130:588–597.
58. Wozar F, Seitz I, Reichel F, Fischer MD. Importance of nonhuman primates as a model system for gene therapy development in ophthalmology. *Klin Monbl Augenheilkd.* 2022;239:270–274.
59. Kay CN, Khanani AM, Hershberger VS, et al. Interim results for the phase 1/2 PRISM trial evaluating 4D-150, a dual-transgene intravitreal genetic medicine for with neovascular (wet) age-related macular degeneration. Presented at the *41st Annual Meeting of the American Society of Retina Specialists. Invest Ophthalmol Vis Sci.* 2023;64:5055.
60. Khanani AM, Hu A, Eichenbaum DA, et al. First interim results (24 weeks) from the randomized phase 2 dose expansion stage of the PRISM clinical trial evaluating 4D-150 in high need patients with neovascular (wet) age-related macular degeneration. *Presented at the Angiogenesis, Exudation, and Degeneration Symposium*. February 3, 2024. Available at: https://bascompalmerlearn.org/course/view.php?id=1697.
61. Nork TM, Dubielzig RR, Christian BJ, et al. Prevention of experimental choroidal neovascularization and resolution of active lesions by VEGF trap in nonhuman primates. *Arch Ophthalmol.* 2011;129:1042–1052.